GEOPHYSICAL RESEARCH LETTERS, VOL. 35, L23806, doi:10.1029/2008GL035617, 2008

Idealized simulations of aerosol influences on tornadogenesis

David G. Lerach,[1] Brian J. Gaudet,[2] and William R. Cotton[1]

Received 7 August 2008; revised 17 October 2008; accepted 24 October 2008; published 3 December 2008.

[1] Numerical simulations of an idealized supercell thunderstorm were performed to assess effects of increased aerosol concentrations acting as cloud condensation nuclei (CCN) and giant CCN (GCCN) on tornadogenesis. Initial background profiles of CCN and GCCN concentrations were set to represent "clean" continental and aerosol-polluted environments, respectively. With a reduction in warm- and cold-rain processes, the polluted environment produced a longer-lived supercell with a well-defined rear flank downdraft (RFD) and relatively weak forward flank downdraft (FFD) that produced weak evaporative cooling, a weak cold pool, and an EF-1 tornado. The clean environment produced no tornado and was less favorable for tornadogenesis. **Citation:** Lerach, D. G., B. J. Gaudet, and W. R. Cotton (2008), Idealized simulations of aerosol influences on tornadogenesis, *Geophys. Res. Lett.*, *35*, L23806, doi:10.1029/2008GL035617.

1. Introduction

[2] Aerosols, both natural and anthropogenic, impact cloud and precipitation processes by acting as cloud condensation nuclei (CCN) and giant CCN (GCCN). Increasing CCN (GCCN) concentrations tends to inhibit (enhance) the warm-rain process [e.g., *Hobbs et al.*, 1970; *Rosenfeld et al.*, 2002]. *Seifert and Beheng* [2006] showed that higher CCN concentrations in simulated multicell storms led to more supercooled water aloft, yielding stronger updrafts. Likewise, *van den Heever et al.* [2006] performed numerical simulations of ordinary convection, finding that higher CCN concentrations initially enhanced the upward transport of supercooled cloud droplets and associated latent heating and higher GCCN concentrations enhanced mature updraft strength through rapid glaciation. While no studies have yet investigated possible aerosol effects on supercell thunderstorms, *van den Heever and Cotton* [2004] (hereinafter referred to as VC04) and *Gilmore et al.* [2004] (hereinafter referred to as G04) addressed microphysical effects, finding that larger raindrop and hail diameters reduced evaporative cooling and melting rates, producing weaker low-level downdrafts and weaker, shallower cold pools. This suggests a possible link between aerosols and supercell tornadogenesis.

[3] The precise mechanisms of supercell tornadogenesis remain unknown. However, multiple studies suggest that these tornadoes are often linked to the rear flank downdraft (RFD), which can transport vertical vorticity to the surface, baroclinically generate horizontal vorticity, and enhance convergence along gust fronts beneath the updraft [e.g., *Burgess et al.*, 1977; *Davies-Jones and Brooks*, 1993; *Brooks et al.*, 1994; *Markowski*, 2002]. Observational and numerical modeling studies by *Markowski et al.* [2002, 2003], supporting a concept first proposed by *Ludlam* [1963], found that air parcels within RFDs tended to be less negatively buoyant (warmer) in tornadic vs. nontornadic supercells. Tornadic vortices increased in intensity and longevity as downdraft parcel buoyancy increased, because colder parcels were more resistant to lifting. N. Snook and M. Xue (Microphysical Sensitivity of tornadogenesis in high-resolution numerical simulations, submitted to *Geophysical Research Letters*, 2008) extended the work of VC04 and G04 to tornadogenesis, verifying that larger raindrops and hailstones yielded warmer cold pools via reduced evaporative cooling. In addition, the larger hydrometeors, with greater terminal fall-speeds, were not advected as far from the updraft before falling to the ground, reducing areal coverage of precipitation. This positioned the gust front closer to the storm center, permitting vertically-oriented updrafts and vertical alignment of low- and mid-level vertical vorticity. This enhanced low-level vertical stretching, thereby increasing the potential for tornadogenesis.

[4] The goal of this study is to investigate possible aerosol indirect microphysical influences on supercell tornadogenesis. Two numerical simulations of an idealized supercell thunderstorm are performed, differing only in initial background aerosol concentrations, representing "clean" and aerosol-polluted environments, respectively. The simulations are compared to assess which is more favorable for tornadogenesis.

2. Model Setup

[5] This study utilized the Regional Atmospheric Modeling System (RAMS) [*Pielke et al.*, 1992] version 4.3.0 [*Cotton et al.*, 2003]. Three two-way interactive nested model grids were used with horizontal grid spacing of 1000, 333.33, and 111.11 m respectively. The outer-most grid (Grid 1), used for generating convection, had horizontal dimensions of 149 × 149 km. Grid 2, centered over Grid 1 coordinates (49 km, 29 km), had dimensions of 60.33 × 60.33 km and was used to simulate the scale of the supercell environment. Grid 3 was centered over Grid 2 coordinates (4.67 km, 4.67 km) and had horizontal dimensions of 38.44 × 21.78 km. This inner grid was used to assess the evolution of the mesocyclone and any tornadic vortices. This study defined a simulated tornado as a low-level vortex that met the following criteria adapted from *Wicker and Wilhelmson* [1995]: (i) It forms in conjunction with a supercell mesocyclone (ii) It is characterized by highly convergent swirling winds affecting a relatively narrow path, and (iii) The near-surface winds exceed minimum EF-1 intensity (40 m s^{-1}).

[1]Department of Atmospheric Science, Colorado State University, Fort Collins, Colorado, USA.
[2]Department of Meteorology, Pennsylvania State University, University Park, Pennsylvania, USA.

0094-8276/08/2008GL035617$05.00

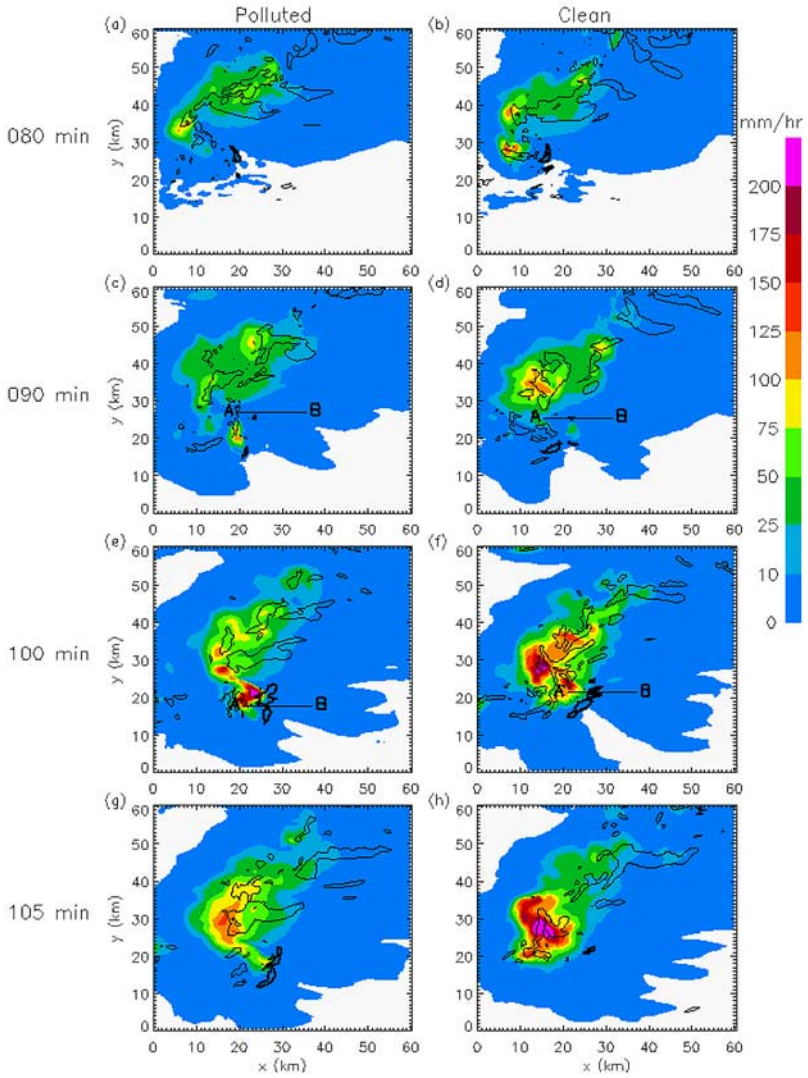

Figure 1. (left) POL and (right) CLN surface precipitation rate on Grid 2 overlaid with vertical velocity at 2 km: updrafts greater than 20 m s^{-1} (thick) and downdrafts greater than 5 m s^{-1} (thin). All x-y axis labels are grid-relative.

[6] A bin-emulating, two-moment bulk microphysics scheme [*Saleeby and Cotton*, 2004] was utilized in these simulations, which included a microphysical category of large cloud droplets with diameters from 40 to 80 μm (cloud2) to better represent the frequently bimodal distribution of cloud droplet spectra. The scheme explicitly predicted mixing ratios and number concentrations of pristine ice, snow, aggregates, graupel, hail, cloud and cloud2 droplets, and rain. Nucleation by CCN, GCCN, and ice nuclei (IN) were explicitly considered. CCN (GCCN) directly nucleated to form cloud (cloud2) droplets. The model excluded the effects of terrain, surface fluxes, surface drag, radiation, and friction due to the time scales and the desire to simplify the experiment. Convection was explicitly resolved on all grids.

[7] The initial sounding utilized was one found to generate storm-splitting and supercells (e.g., VC04); this study focused on the right-mover. Convection was initiated by introducing a "warm bubble" (10 × 10 × 1.5 km, 2 K thermal perturbation, 20% moisture perturbation) at the surface. The model aerosol species were initially horizontally-homogeneous with prescribed vertical profiles of CCN, GCCN, and IN concentrations. In one simulation, initial background aerosol concentration profiles were set for a relatively "clean" continental environment (CLN). In the other, concentrations were increased to act as an aerosol-polluted environment (POL) due to dust or pollutants. CCN (GCCN) concentrations near the surface were set to 600 (0.06) cm^{-3} and 2000 (0.2) cm^{-3} for the CLN and POL simulations, respectively, based on CRYSTAL-FACE measurements [*van den Heever et al.*, 2006]. The initial IN profile was held fixed between simulations; IN effects will not be addressed in this study. Simulations lasted two hours. Grid 2 (3) was spawned at 60 (85) min.

3. Results

[8] Figure 1 displays the time evolution of Grid 2 precipitation rate for both simulations. Updrafts (downdrafts) greater than 20 (5) m s^{-1} at 2 km are overlaid. For simplicity the positive "y", negative "y", positive "x", and negative "x" directions will be referred to as north, south, east, and

west, respectively. By 80 min, a pronounced hook-shaped structure has formed on the southern end of each storm that wraps cyclonically around the main updraft, associated with the RFD. Precipitation rates greater than 10 mm hr^{-1} generally lie within downdrafts greater than 5 m s^{-1}. The POL hook is more defined. However, the CLN supercell shows the strongest precipitation rates, with values greater than 100 mm hr^{-1} in the RFD and forward flank downdraft (FFD). While precipitation rates greater than 100 mm hr^{-1} exist toward the rear of the POL RFD, maximum values in the FFD only reach 70 mm hr^{-1}. The hook-like structure is less defined at 90 min in both storms, though that of the POL supercell is more pronounced. Precipitation intensity evolves differently between the two storms after this time. The POL storm exhibits a distinct maximum in precipitation rate in the RFD just behind the main updraft. Precipitation rates are strengthening in the core of the CLN FFD but weakening within the dissipating RFD. The CLN FFD still contains significantly heavier precipitation rates than the POL case. At 100 min, the POL supercell maintains a well-defined RFD whereas the CLN RFD has essentially dissipated, leaving only a large FFD containing heavy rain with precipitation rates greater than 200 mm hr^{-1}. As the CLN updraft continues to move ahead of the rest of the system, the POL updraft remains adjacent to the precipitation-filled RFD, now showing precipitation rates greater than 200 mm hr^{-1}. The POL case exhibits maximum precipitation rates in the southern portion of the RFD while the CLN case continues to show maximum rates further to the north. At 105 min, the POL case maintains a well-defined hook and a large region of updrafts greater than 20 m s^{-1} at 2 km. The POL RFD weakens as the storm′s FFD produces most of the precipitation, with maximum precipitation rates near 150 mm hr^{-1}. The CLN supercell continues to dissipate, showing a single core of FFD precipitation and only remnants of a low-level updraft. The CLN case continues to produce the highest precipitation rates (>200 mm hr^{-1}).

[9] The POL simulation produces a steadier, longer-lived storm while the CLN simulation produces heavier rainfall. At 120 min, the pattern of total accumulated precipitation on Grid 2 (not shown) in the POL case exhibits two distinct precipitation maxima greater than 50 mm associated with the storm′s RFD and FFD. That of the CLN case shows only a single maximum greater than 65 mm, associated with the FFD (resembling precipitation rate patterns in Figures 1g and 1h). Notice that the FFD in the CLN simulation strengthens near 90 min, overtaking the RFD (Figure 1d). At 100 min the POL supercell produces a tornado-like vortex of EF-1 intensity, unlike the CLN supercell. Figure 2 displays near-surface pressure, vertical vorticity, horizontal winds, and potential temperature on Grid 3 for both simulations at 100 min over the POL low-level mesocyclone. The POL case shows the distinct formation of a strong low-pressure center of 989 mb associated with the tornado. Pressure increases rapidly north and south of the low, signifying the RFD- and FFD-based gust fronts. The CLN simulation attempts to create a similar pressure pattern. However, by 100 min the pressure center has weakened, leaving only a single line of relatively high pressure (>995 mb) associated with a single gust front. The POL supercell produces a well-defined positive vertical vorticity center and cyclonic winds, associated with the tornadic vortex. An 'S'-shaped pattern in the vorticity field

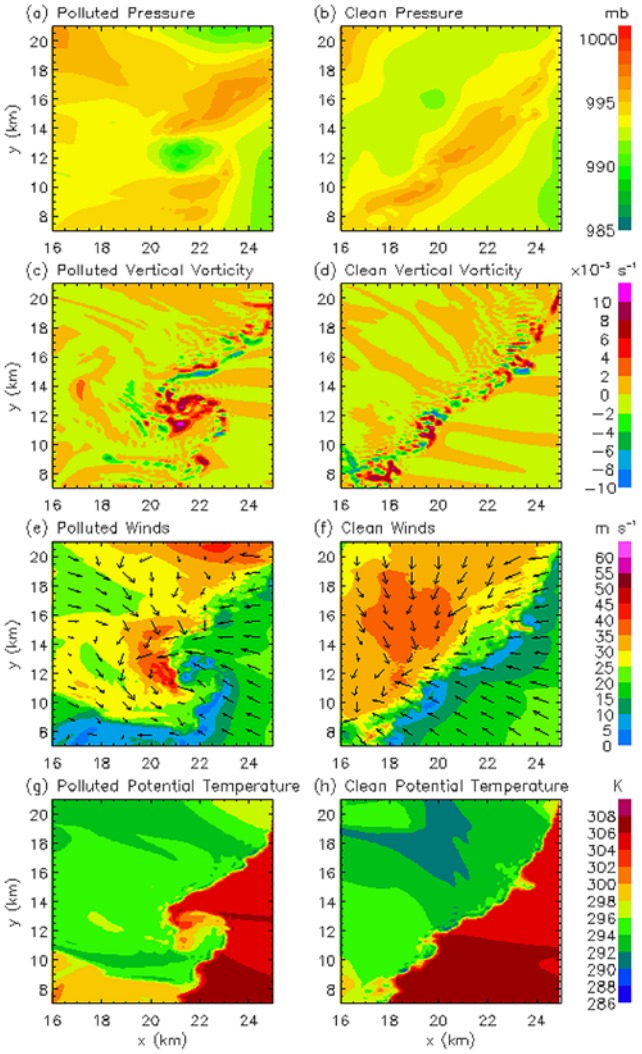

Figure 2. Grid 3 near-surface (24 m) pressure, vertical vorticity, horizontal winds overlaid with directional wind barbs, and potential temperature for the (left) POL and (right) CLN simulations at 100 minutes.

signifies the advancing gust front immediately south associated with the RFD and the FFD-based gust front to the north, both associated with confluent winds. The strongest near-surface winds exceed 45 m s^{-1} where the tangential winds due to vortex rotation coincide with the supercell propagation direction. Unable to create a tornado, the CLN supercell produces a single, relatively straight gust front with confluent winds (maximum winds ~35 m s^{-1} behind the gust front) and alternating pockets of positive and negative vertical vorticity.

[10] Ice and raindrop size distributions were compared between simulations to assess aerosol microphysical effects on precipitation. The POL case produced significantly more hailstones and small ice crystals, but of smaller sizes as those in the CLN case. More ice was transported to the anvil in the POL supercell while more ice was available for precipitation processes in the CLN case. One might have expected the POL case to produce the strongest updrafts (via more latent heat release) and largest hailstones [*Foote*, 1984]. However, there were no significant differences in

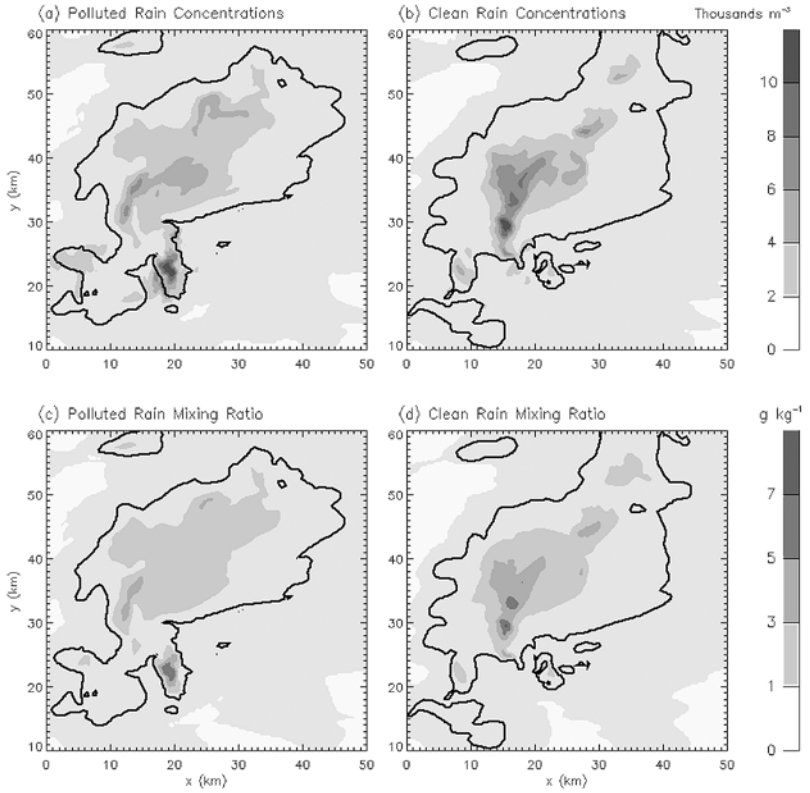

Figure 3. Rain concentrations at 1 km for the (a) POL and (b) CLN simulations and rain mixing ratios at 1 km for the (c) POL and (d) CLN simulations at 90 minutes on Grid 2. Plots are overlaid with 30-dBZ model reflectivity boundaries at 1 km.

updraft strength (70 m s^{-1}) between simulations. The simulations neither produced major differences in raindrop sizes. However, raindrop concentrations varied significantly between simulations with respect to storm location. Figure 3 displays 1-km rain concentrations and rain mixing ratios on Grid 2 at 90 min, overlaid with 30-dBZ model reflectivity boundaries at 1 km to present a relative sense of storm position. Maximum concentrations were similar between cases (CLN: 13000 vs. POL: 12000 m^{-3}). However, the highest concentrations in the POL supercell existed within the RFD while those of the CLN were in the FFD, as the RFD had nearly dissipated by this time. This translated to higher rain mixing ratios within the CLN FFD region.

[11] The enhanced aerosol concentrations in the POL case resulted in a reduction in warm-rain processes producing numerous, small cloud droplets as compared to the CLN simulation. Larger amounts of supercooled drops were lofted in the updraft to act as embryos for ice formation, yielding many small ice particles that were eventually lofted into the storm′s anvil. The CLN supercell, which produced larger ice particles with greater terminal fall speeds, produced more ice used in cold-rain processes, leading to heavier precipitation rates in the CLN FFD compared to the POL case. The greater evaporative cooling rates associated with higher rainfall rates caused the FFD to surge out in the CLN simulation and destroy the RFD at the rear of the storm. Potential temperature at 24 m at the time of POL tornado vortex occurrence (Figures 2g and 2h) shows that the minimum cold pool temperatures were similar between simulations. However, the POL cold pool remained approximately 2 K warmer near the developed vortex as compared to the CLN case, where the cold pool extended all the way to the storm′s gust front. The stronger cold pool in the CLN storm hindered any vortex formation by advancing the gust front further away from the storm′s core, thus locating the low-level updraft and vorticity source further away from the low-level mesocyclone compared to the POL case. While implied in Figure 1, this is more evident in Figure 4, which shows vertical cross-sections of vertical vorticity through the main updrafts of each simulation at 90 and 100 min. At 90 min, concentrated positive vertical vorticity greater than 25×10^{-3} s^{-1} was present within the low-level mesocyclone near 2 km as well as near the surface in both simulations. However, by 100 min the POL supercell exhibited a column of strong vertical vorticity extending from the low-level mesocyclone to the surface. The CLN case failed to create such a column. The near-surface vertical vorticity at 90 min was located nearly 5 km further east from the vertical vorticity associated with the low-level mesocyclone in the CLN simulation.

4. Discussion

[12] This study presented a preliminary look at possible effects of dust and pollutant aerosol acting as CCN and GCCN on supercell storms. Enhanced aerosol concentrations in the POL simulation reduced warm- and cold-rain processes within the RFD and FFD, resulting in lower precipitation rates. A relatively weak cold pool was produced at the updraft-downdraft interface due to low evap-

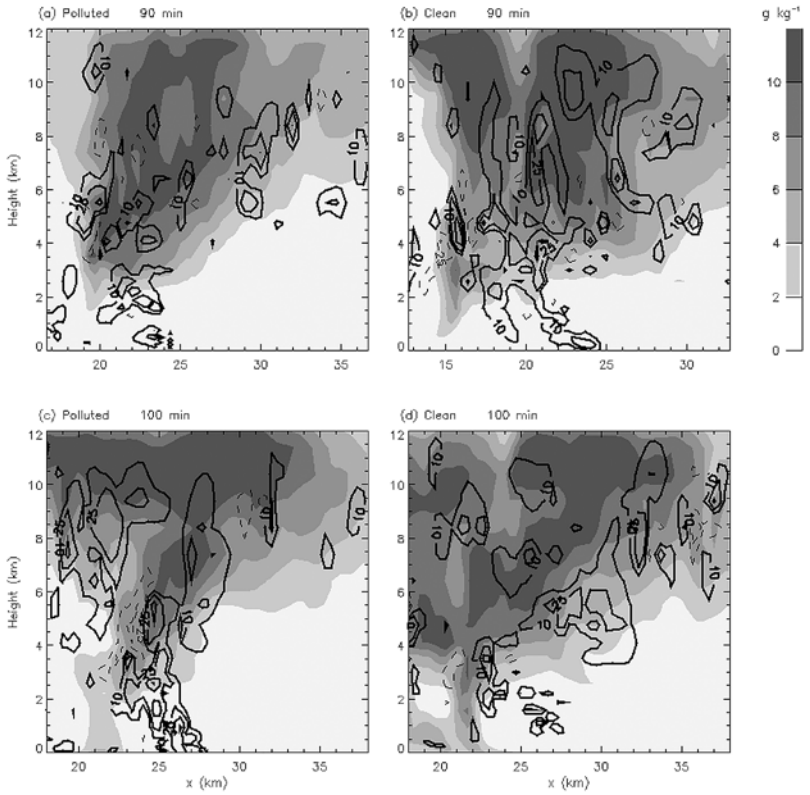

Figure 4. Constant 'y' vertical cross-sections of total mixing ratio overlaid with vertical vorticity (-25, -10, 10, 25, 50 $\times$ 10^{-3} s^{-3}) at (top) 90 and (bottom) 100 minutes on Grid 2 through the main updraft for the (left) POL and (right) CLN simulations. Cross-section regions are denoted in Figure 1 as lines 'AB'.

orative cooling rates, providing a favorable environment for tornadogenesis, where the low-level mesocyclone and near-surface vorticity provided by the RFD-based gust front remained vertically-stacked. This resulted in the formation of an EF-1 tornado while the CLN case failed to produce such a vortex. Heavier precipitation in the RFD and FFD in the CLN simulation produced more evaporative cooling, and thus a stronger surface cold pool that surged and destroyed the RFD structure. This resulted in a single gust front that advected away more rapidly from the storm system, separating the low-level vorticity source from the parent storm and thus hindering the tornadogenesis process. Studies such as *Weisman and Klemp* [1982] and *Brooks et al.* [1994] found similar potential failure mechanisms. The results were consistent with the findings of *Markowski et al.* [2002, 2003] and Snook and Xue (submitted manuscript, 2008) regarding the importance of cold pool dynamics and the vertical alignment of vertical vorticity within a supercell to tornadogenesis. The key difference between the results of this study and Snook and Xue (submitted manuscript, 2008) was the mechanism controlling evaporative cooling within downdrafts and thus cold pool strength (rain amount vs. rain and hail size, respectively). Nonetheless, this single, idealized study found that "other things being equal", a polluted environment is more favorable for tornadogenesis. However, multiple factors control cold pool strength including surface fluxes of heat and water vapor [*Ross et al.*, 2004], storm-relative midlevel flow [e.g., *Brooks et al.*, 1994], convective available potential energy (CAPE) [*Markowski et al.*, 2002] and microphysics, particularly hail (VC04) and raindrop size (G04). Furthermore, additional work is needed to address the robustness of the results presented.

[13] **Acknowledgments.** Thanks to the late Ed Danielson, whose work in Project DUSTORM first suggested aerosols might influence tornadic thunderstorms, Louie Grasso (CIRA) for his insight regarding this work, and Susan van den Heever (CSU), who supplied aerosol concentration profiles used in this study. This work was funded by National Science Foundation (NSF) grant ATM-0638910.

References

Brooks, H. E., C. A. Doswell III, and R. B. Wilhelmson (1994), The role of midtropospheric wind in the evolution and maintenance of low-level mesocyclones, *Mon. Weather Rev.*, *122*, 126–136.

Burgess, D. W., R. A. Brown, L. R. Lemon, and C. R. Safford (1977), Evolution of a tornadic thunderstorm, paper presented at the 10th Conference on Severe Local Storms, Am. Meteorol. Soc., Omaha, Nebr.

Cotton, W., et al. (2003), Rams 2001: Current status and future directions, *Meteorol. Atmos. Phys.*, *82*, 5–29.

Davies-Jones, R. P., and H. E. Brooks (1993), Mesocyclogenesis from a theoretical perspective, in *The Tornado: Its Structure, Dynamics, Prediction, and Hazards, Geophys. Monogr. Ser.*, vol. 79, edited by C. Church et al., pp. 105–114, AGU, Washington, D. C.

Foote, G. B. (1984), A study of hail growth utilizing observed storm conditions, *J. Clim. Appl. Meteorol.*, *23*, 84–101.

Gilmore, M. S., J. M. Straka, and E. N. Rasmussen (2004), Precipitation uncertainty due to variations in precipitation particle parameters within a simple microphysics scheme, *Mon. Weather Rev.*, *132*, 2610–2627.

Hobbs, P. V., L. F. Radke, and S. E. Shumway (1970), Cloud condensation nuclei from industrial sources and their apparent influence on precipitation in Washington State, *J. Atmos. Sci.*, *27*, 81–89.

Ludlam, F. H. (1963), Severe local storms: A review, in *Severe Local Storms, Meteorol. Monogr.*, vol. 27, pp. 1–30, Am. Meteorol. Soc., Boston, Mass.

Markowski, P. M. (2002), Hook echoes and rear-flank downdrafts: A review, *Mon. Weather Rev.*, *130*, 852–876.

Markowski, P. M., J. M. Straka, and E. N. Rasmussen (2002), Direct surface thermodynamic observations within the rear-flank downdrafts of nontornadic and tornadic supercells, *Mon. Weather Rev.*, *130*, 1692–1721.

Markowski, P. M., J. M. Straka, and E. N. Rasmussen (2003), Tornadogenesis resulting from the transport of circulation by a downdraft: Idealized numerical simulations, *J. Atmos. Sci.*, *60*, 795–823.

Pielke, R. A., et al. (1992), A comprehensive meteorological modeling system–RAMS, *Meteorol. Atmos. Phys.*, *49*, 69–91.

Rosenfeld, D., R. Lahav, A. Khain, and M. Pinsky (2002), The role of sea spray in cleansing air pollution over ocean via cloud processes, *Science*, *297*, 1667–1670.

Ross, A. N., A. M. Tompkins, and D. J. Parker (2004), Simple models of the role of surface fluxes in convective cold pool evolution, *J. Atmos. Sci.*, *61*, 1582–1595.

Saleeby, S. M., and W. R. Cotton (2004), A large droplet mode and prognostic number concentration of cloud droplets in the Colorado State University Regional Atmospheric Modeling System (RAMS). Part I: Module descriptions and supercell test simulations, *J. Appl. Meteorol.*, *43*, 182–195.

Seifert, A., and K. D. Beheng (2006), A two-moment cloud microphysics parameterization for mixed-phase clouds. Part 2: Maritime vs. continental deep convective storms, *Meteorol. Atmos. Phys.*, *92*, 67–82.

van den Heever, S. C., and W. R. Cotton (2004), The impact of hail size on simulated supercell storms, *J. Atmos. Sci.*, *61*, 1596–1609.

van den Heever, S. C., G. G. Carrio, W. R. Cotton, and P. J. DeMott (2006), Impacts of nucleating aerosol on Florida storms. Part I: Mesoscale simulations, *J. Atmos. Sci.*, *63*, 1752–1775.

Weisman, M. L., and J. B. Klemp (1982), The dependence of numerically simulated convective storms on vertical wind shear and buoyancy, *Mon. Weather Rev.*, *110*, 504–520.

Wicker, L. J., and R. B. Wilhelmson (1995), Simulation and analysis of tornado development and decay within a three-dimensional supercell thunderstorm, *J. Atmos. Sci.*, *52*, 2675–2703.

W. R. Cotton and D. G. Lerach, Department of Atmospheric Science, Colorado State University, Fort Collins, CO 80523, USA. (dlerach@atmos.colostate.edu)

B. J. Gaudet, Department of Meteorology, Pennsylvania State University, University Park, PA 16802, USA.